

Vision–Language Enhanced Foundation Model for Semi-supervised Medical Image Segmentation

Jiaqi Guo^{1*} Mingzhen Li^{1*} Hanyu Su^{2*} Santiago López¹ Lexiaozi Fan³
 Daniel Kim³ Aggelos Katsaggelos^{1†}

¹ECE, Northwestern University ²Stats, Northwestern University ³Radiology, Northwestern University

Abstract

Semi-supervised learning (SSL) has emerged as an effective paradigm for medical image segmentation, reducing the reliance on extensive expert annotations. Meanwhile, vision–language models (VLMs) have demonstrated strong generalization and few-shot capabilities across diverse visual domains. In this work, we integrate VLM-based segmentation into semi-supervised medical image segmentation by introducing a Vision–Language Enhanced Semi-supervised Segmentation Assistant (VESSA) that incorporates foundation-level visual–semantic understanding into SSL frameworks. Our approach consists of two stages. In Stage 1, the VLM-enhanced segmentation foundation model VESSA is trained as a reference-guided segmentation assistant using a template bank containing gold-standard exemplars, simulating learning from limited labeled data. Given an input–template pair, VESSA performs visual feature matching to extract representative semantic and spatial cues from exemplar segmentations, generating structured prompts for a SAM2-inspired mask decoder to produce segmentation masks. In Stage 2, VESSA is integrated into a state-of-the-art SSL framework, enabling dynamic interaction with the student model: as student predictions become more refined, they are fed back to VESSA as prompts, allowing it to generate higher-quality pseudo-labels and stronger guidance. Extensive experiments across multiple segmentation datasets and domains show that VESSA-augmented SSL significantly enhances segmentation accuracy, outperforming state-of-the-art baselines under extremely limited annotation conditions.

1. Introduction

Accurate delineation of anatomical structures and pathological regions in medical images underpins computer-assisted diagnosis, treatment planning, and longitudinal dis-

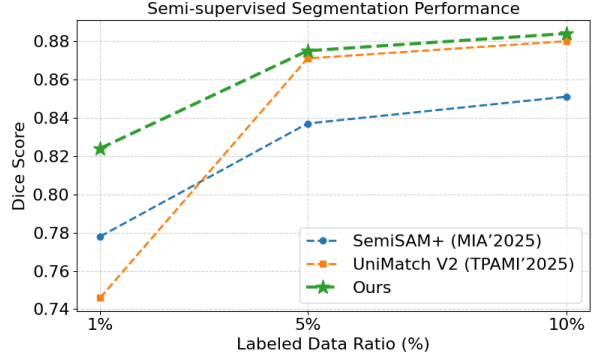


Figure 1. Comparison of segmentation performance (Dice score) between our method and two recent state-of-the-art approaches on the ACDC dataset under different labeled data ratios.

ease monitoring [22, 41]. Deep learning–based segmentation can achieve high accuracy when large, well-annotated datasets are available, but such datasets are scarce in practice: public and institutional collections often provide only sparse or task-specific labels, and expert annotation is costly and difficult to scale [3, 12, 28, 35]. This mismatch has sharpened the demand for segmentation frameworks that remain accurate under limited supervision and can generalize across modalities and clinical domains [20, 30, 42, 45]. Semi-supervised medical image segmentation addresses this gap by combining a small labeled set with abundant unlabeled images [9]. Classical frameworks rely on pseudo-labeling, consistency regularization, and teacher–student architectures to transfer supervision from labeled to unlabeled data [37, 44]. While these methods are fully automated and yield highly precise segmentations within a given dataset once trained, they are tuned per dataset and per task, with weak generalization [20, 25, 45]. Moreover, consistency-based methods are prone to confirmation bias: teacher and student often share the same architecture and supervise each other only through perturbed versions of their own predictions, so erroneous pseudo-labels tend to be amplified rather

*Equal contributions.

†Corresponding author.

than corrected in the absence of external guidance [2, 6, 16]. Segmentation foundation models have recently emerged as an alternative route to generalization [32, 53]. The Segment Anything Model (SAM) [15], for example, can produce masks in a few-shot or even zero-shot manner from user prompts such as points, boxes, or coarse masks, and exhibits strong cross-domain robustness. However, these models are not fully automated, as high-quality results typically require careful, case-by-case prompt engineering by human users [46, 48]. In addition, they usually do not explicitly exploit unlabeled data for fine-tuning.

More recently, vision–language assisted segmentation models such as LISA [17] begin to bridge language supervision and pixel-level prediction by mapping textual descriptions directly to segmentation masks. Conditioning on text removes the need for per-image location prompts and offers flexible semantic control [17, 24, 53]. Yet existing vision–language models are largely trained on natural images, and thus struggle with domain shift to medical data and with capturing the fine-grained semantic and structural cues required in clinical practice [40, 47]. This highlights the need for a vision–language–driven segmentation foundation model tailored to medical imaging, trained on diverse datasets spanning CT, MRI, ultrasound, X-ray, and multiple anatomical and pathological targets, and made broadly available to the community.

In this work, we propose **VESSA** (Vision–Language Enhanced Semi-supervised Medical Segmentation Assistant), an end-to-end foundation model that combines vision–language learning with classical semi-supervised segmentation. Trained on seven public medical datasets spanning various modalities and clinical domains, VESSA adopts a template-based training paradigm: a small set of annotated images, stored in a template bank, guides segmentation for unlabeled data. Our architecture extends the Qwen3-VL [38] vision–language backbone with a template retrieval mechanism and a memory-augmented segmentation module. For each input image, the most anatomically relevant template is retrieved from a bank using DINOv2 [31] features. The input image, its matched template, and a descriptive text prompt are jointly processed by Qwen3-VL, which generates a detailed representation and a dedicated segmentation token. This token is transformed into a continuous prompt to guide the mask decoder. At the same time, visual features and the mask from the retrieved template are stored in a memory bank and integrated into decoding, enabling precise structural guidance from the template.

Once pre-trained, VESSA can be plugged in as an automatic annotator within standard semi-supervised segmentation pipelines. For a new task with limited labeled data, these examples initialize the template bank. VESSA then generates high-quality pseudo-labels on unlabeled data via

class-aware prompting. As the downstream model improves, its predictions are fed back into VESSA as additional prompts, forming a closed-loop annotator that co-evolves with the model. Figure 1 compares VESSA with SemiSAM+ and Unimatch v2 on the ACDC dataset under different label ratios.

In summary, this paper makes the following contributions.

- We introduce VESSA, a medical vision–language segmentation foundation model trained with a reference-based prompting mechanism and a template-embedded memory design. VESSA is trained to emulate the setting where a small bank of gold-standard template images is available, and it is trained with 7 large public medical challenge datasets that cover multiple modalities and clinical domains.
- We propose a principled pipeline to integrate VESSA into standard semi-supervised medical image segmentation frameworks, exploiting its template bank and memory mechanisms during inference to provide strong supervision from limited labels. Our empirical results show that this integration significantly improves the performance of the baseline on multiple public benchmarks, advancing the state of the art in semi-supervised medical image segmentation.

2. Related Works

2.1. Semi-supervised Medical Image Segmentation

Semi-supervised learning has emerged as a promising paradigm in medical image analysis, addressing the scarcity of expert-annotated data by leveraging both labeled and unlabeled samples for model training [9, 20, 25, 41, 42, 45]. The two commonly adopted strategies for leveraging unlabeled data are pseudo-labeling [2, 7, 10, 11, 20, 36, 45], which assigns model-generated labels to unlabeled images to expand the training set but is sensitive to early prediction noise, and consistency learning [18, 25, 29, 37, 39], which enforces prediction stability under various perturbations to improve robustness but depends heavily on the quality of the supervising signals.

Semi-supervised learning for medical image segmentation has generally followed the same principles as in natural-image SSL, relying on pseudo-labeling, consistency regularization, and teacher–student architectures. Early efforts explored adversarial training [8, 11] to refine pseudo-labels or to align the prediction distributions between labeled and unlabeled data. More recent advances have focused on two major directions.

Weak-to-strong consistency. UniMatch [42] revisits FixMatch-style [36] consistency for semantic segmentation by using predictions from weakly augmented views to supervise strongly augmented ones, achieving substantial improvements on both natural and medical

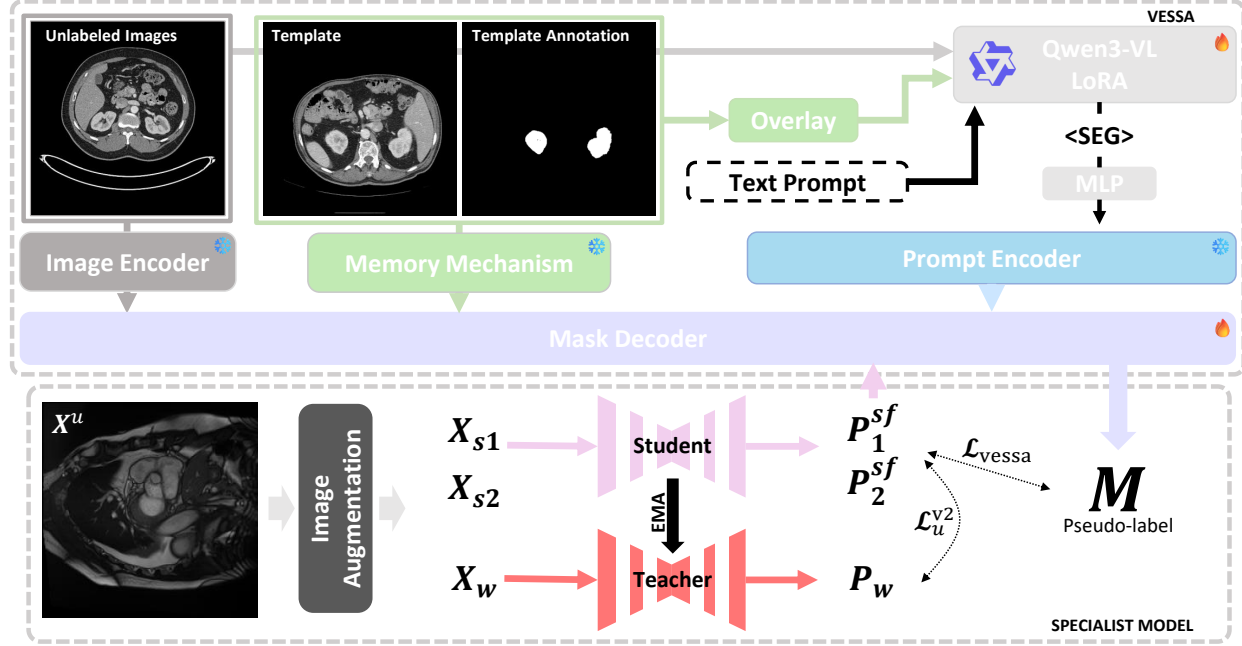


Figure 2. **Overview of our model.** (a) **VESSA:** During training, an input image, its matched template overlay, and a reference text describing the image-template pair are fed into the VLM (Qwen3-VL). The generated text containing the `<SEG>` token is mapped by an MLP to a prompt embedding for the prompt encoder of the segmentation foundation model, while the matched template and its annotations are stored in the model’s memory bank for mask prediction. (b) **Specialist Model:** A student-teacher network applies weak and strong augmentations to enforce consistency on each input image, while VESSA provides additional pseudo-label supervision. In later training stages, student predictions are fed back to VESSA to refine its pseudo-labels by supplying spatial and localization cues to VESSA’s mask decoder.

datasets. UniMatch-V2 [43] further upgrades the encoder to ViT/DINOv2 [31] and simplifies the augmentation pipeline, showing that stronger backbones coupled with streamlined consistency can push semi-supervised performance even further.

Multi-perspective consistency and uncertainty modeling. Recent medical SSL approaches [23, 49, 50, 52] incorporate multi-view or multi-scale consistency constraints, adversarial perturbations, and uncertainty-aware regularization to improve robustness under scarce annotations, enabling models to extract more reliable supervisory signals from unlabeled data.

2.2. Segmentation with Foundation Models

Promptable segmentation foundation models. The Segment Anything Model (SAM) [15] and its successor SAM2 [34] introduced promptable segmentation at scale, leveraging billions of masks to generalize across diverse visual domains. Given sparse prompts such as points or bounding boxes, SAM produces high-quality masks, while SAM2 extends this capability to both images and videos through an improved memory mechanism. These models have also been adapted to medical imaging, where variants such as MedSAM [27] and ultrasound-specific derivatives

fine-tune SAM on modality-specific data. However, despite strong cross-domain generalization, promptable foundation models still rely on explicit per-case prompts (typically provided by human users) and are trained primarily in fully supervised regimes, limiting their applicability in semi-supervised medical segmentation.

SAM in semi-supervised medical segmentation. SemiSAM [49] explores SAM as an auxiliary pseudo-labeler within semi-supervised medical image segmentation. A specialist segmentation network first produces localization cues (e.g. points or boxes), which are then passed to SAM; the resulting masks are used as additional supervision signals, generating substantial gains when only 1–4 labeled images are available. SemiSAM+ [50] extends this idea into a more general foundation model–driven SSL framework, investigating how SAM variants can be incorporated into mean-teacher-style pipelines. Despite these advances, SAM’s strong sensitivity to prompt quality remains a bottleneck: noisy early-stage predictions from the student network can result in sub-optimal prompts and degraded pseudo-labels.

Vision-language segmentation assistants. LISA [17] equips a multimodal large language model (MLLM) with a dedicated `<SEG>` token whose embedding is decoded

into a segmentation mask, demonstrating that an MLLM can jointly reason over language and visual content to generate dense pixel-level outputs. By relying solely on text prompts that specify semantic classes, LISA sidesteps the need for per-sample spatial prompts and significantly reduces manual effort. However, trained entirely on natural images, LISA transfers poorly to medical segmentation, particularly when faced with modality-specific appearance patterns and clinical terminology.

Reference-based medical vision–language models. In the medical domain, RAU [21] is the first to demonstrate reference-based anatomical understanding with a vision–language model (VLM), integrating SAM2 as the segmentation backend. RAU trains the VLM with visual question answering and bounding-box prediction tasks to instill spatial reasoning capabilities, which are then used to initialize SAM2’s memory and enable precise segmentation of small anatomical structures.

VESSA is inspired by LISA and RAU but is tailored specifically for semi-supervised medical segmentation. First, VESSA is pretrained across seven public medical benchmarks spanning multiple modalities and clinical tasks, enabling broad anatomical coverage. Second, its interface is designed for seamless plug-in use within semi-supervised pipelines, where VESSA acts as a stable pseudo-label generator driven by template-based reference guidance rather than fragile, hand-crafted prompts.

3. Method

Overview. Our pipeline comprises two stages, as shown in Figure 2. In **Stage 1**, we pretrain the vision–language foundation model **VESSA** on a large-scale medical imaging dataset (Section 3.1). In **Stage 2**, under a semi-supervised setting with limited labeled data, VESSA is integrated into a semi-supervised framework to enhance supervision and improve segmentation performance. The complete framework is described in Section 3.2.

3.1. Pre-training of VESSA

We pretrain **VESSA** end-to-end on seven public medical segmentation datasets spanning various modalities and clinical domains. The training paradigm is designed to mirror semi-supervised settings by leveraging a template-based input construction strategy that enriches visual and textual context.

Template Bank and Reference-Based Prompt. Each input to the vision–language backbone of VESSA is constructed using three elements: an input image x_{img} , a reference template image x_{temp} , and a reference text prompt $y_{\text{text}}^{\text{in}}$.

To simulate a semi-supervised scenario, we randomly select 5% of labeled samples (by patient) from each dataset to form a *template bank*. Each template image x_{temp}^i is en-

coded using DINOV2 [31] to obtain a feature embedding f_i , resulting in pairs $\{(f_i, x_{\text{temp}}^i)\}$. During training, for a given input image, we extract its feature f_{img} and compute cosine similarity with each template feature as $s_i = \cos(f_{\text{img}}, f_i)$. Rather than naively selecting the top-1 match, we adopt a softmax sampling strategy over the top-3 candidates:

$$P(x_{\text{temp}}^i) = \frac{\exp(s_i/\tau)}{\sum_{j \in \mathcal{T}_{\text{top3}}} \exp(s_j/\tau)}, \quad (1)$$

where τ is a temperature hyperparameter and $\mathcal{T}_{\text{top3}}$ denotes the set of the three most similar templates, enabling diversity while maintaining relevance.

The selected template image x_{temp} is augmented and overlaid with its binary segmentation mask. Augmentation details are provided in the supplementary material. Simultaneously, a reference text prompt is sampled from a predefined prompt bank with diverse template instructions; an example prompt is: “I’ve provided two images: the target image and a reference image with a segmentation mask highlighted in green overlay.” These three components together encourage the model to learn spatial and semantic alignment between the input and template. Figure 3 shows two examples of the prompt sent to VESSA and VESSA’s prediction during the training.

Text-to-Mask Embedding Conversion. The VLM generates a text output $\hat{y}^{\text{txt}} = F_{\text{VLM}}(x_{\text{img}}, x_{\text{overlay}}, y_{\text{text}}^{\text{in}})$. We adopt the embedding-as-mask strategy inspired by LISA. Specifically, we expand the vocabulary of the VLM to include a special token $\langle \text{SEG} \rangle$, and apply an MLP projection to the final-layer embedding corresponding to this token, i.e., $h_{\text{seg}} = \text{MLP}(\text{Emb}_{\text{VLM}}(\langle \text{SEG} \rangle))$.

In parallel, we extract image features from SAM2’s vision encoder [34], denoted $f_{\text{img}} = E_{\text{vision}}(x_{\text{img}})$. These two components are then fused via the SAM2 prompt encoder to generate a prompt embedding: $p = E_{\text{img}}(h_{\text{seg}}, f_{\text{img}})$.

Template-Driven Memory Encoding. The selected template x_{temp} and its corresponding binary mask m_{temp} are passed to the memory encoder of SAM2 to compute memory features $f_{\text{memory}} = E_{\text{memory}}(x_{\text{temp}}, m_{\text{temp}})$. These features interact with f_{img} through a cross-attention mechanism: $q = \text{Attention}(f_{\text{img}}, f_{\text{memory}})$. Finally, both the prompt embedding p and attention output q are sent to the mask decoder to generate the predicted segmentation: $m_{\text{pred}} = D_{\text{mask}}(p, q)$. This ensures that template guidance influences both the prompting and decoding stages.

Training Objective. VESSA is trained with a multi-task loss that supervises both text generation and segmentation:

Target Image	User Instructions	Template	VESSA Pred + Overlay
	Segment the target image following the reference segmentation pattern (green overlay).		
	Apply the segmentation pattern from the template (green overlay) to the target image.		

Figure 3. **Three-component prompts sent to VESSA:** From left to right, the target image, the text prompt, and a template sample used to guide the segmentation. The templates are automatically selected through a matching mechanism. The two images on the right show the output segmentation (binary mask & overlay).

$$\mathcal{L} = \lambda_{\text{txt}} \left[- \sum_{t=1}^T \log P(\hat{y}_t^{\text{txt}} = y_t^{\text{txt}}) \right] + \lambda_{\text{mask}} \cdot \mathcal{L}_{\text{mask}}, \quad (2)$$

The overall mask loss $\mathcal{L}_{\text{mask}}$ consists of a Dice loss term that ensures overlap consistency, and a binary cross-entropy (BCE) term that captures pixel-level correctness:

$$\mathcal{L}_{\text{mask}} = \lambda_{\text{dice}} \left[1 - \frac{2 \sum_{i=1}^N m_i \hat{m}_i}{\sum_{i=1}^N m_i + \sum_{i=1}^N \hat{m}_i + \epsilon} \right] + \lambda_{\text{bce}} \left[-\frac{1}{N} \sum_{i=1}^N (m_i \log(\hat{m}_i) + (1 - m_i) \log(1 - \hat{m}_i)) \right]. \quad (3)$$

Here, \hat{y}_t^{txt} denotes the predicted token at timestep t , and m_i , \hat{m}_i are the ground-truth and predicted segmentation logits for pixel i respectively. The coefficients λ_{txt} , λ_{mask} , λ_{dice} and λ_{bce} control the contribution of each term, and ϵ is a small constant for numerical stability.

3.2. VESSA in Semi-Supervised Medical Image Segmentation

Preliminaries. We choose UniMatch v2 [43] as our task-specific semi-supervised segmentation model, which itself is a simplified and more efficient variant of FixMatch [36] with unified image–feature augmentations and dual strong views. We consider a labeled set $\mathcal{D}_l = \{(x_i^l, y_i^l)\}$ and an unlabeled set $\mathcal{D}_u = \{x_i^u\}$, where x_i^l and x_i^u denote labeled and unlabeled input images, respectively, and y_i^l is the corresponding ground-truth mask for labeled samples. For labeled data, UniMatch v2 uses the standard segmentation loss that combines pixel-wise cross-entropy and Dice loss.

Given a mini-batch of B_l labeled samples, the supervised loss is

$$\mathcal{L}_{\text{sup}} = \lambda_{\text{ce}} \left[-\frac{1}{B_l} \sum_{i=1}^{B_l} y_i^l \log(\hat{y}_i^l) \right] + \lambda_{\text{dice}} \left[1 - \frac{2 \sum_{i=1}^{B_l} y_i^l \hat{y}_i^l}{\sum_{i=1}^{B_l} y_i^l + \sum_{i=1}^{B_l} \hat{y}_i^l + \epsilon} \right], \quad (4)$$

where $\hat{y}_i^l = f_{\theta_s}(x_i^l)$ is the prediction of the student network f_{θ_s} .

For each unlabeled image x^u , UniMatch v2 first generates a weakly augmented view $x_w = A_w(x^u)$ and two strongly augmented views $x_{s1} = A_s(x_w)$ and $x_{s2} = A_s(x_w)$. An exponential moving average(EMA) [37] teacher network f_{θ_t} produces a prediction on the weak view, $p_w = f_{\theta_t}(x_w)$, from which a hard pseudo label $\hat{p}_w = \arg \max_c p_{w,c}$ is obtained. Only high-confidence pixels with $\max_c p_{w,c} \geq \tau$ are used via an indicator function $\mathbb{I}_i = \mathbf{1}(\max_c p_{w,i,c} \geq \tau)$. The two strong views are fed into a shared encoder g and decoder h . UniMatch v2 applies complementary channel-wise Dropout on the encoder features: given a binary mask $M \in \{0, 1\}^C$ sampled from a binomial distribution with probability 0.5, the features are perturbed as $e_{s1} \leftarrow g(x_{s1}) \odot M \times 2$ and $e_{s2} \leftarrow g(x_{s2}) \odot (1 - M) \times 2$, and decoded to predictions $p_1^{\text{sf}} = h(e_{s1})$ and $p_2^{\text{sf}} = h(e_{s2})$. The unlabeled loss of UniMatch v2 averages the two strong streams and supervises them with the same weak pseudo label:

$$\mathcal{L}_{\text{u}}^{\text{v2}} = \frac{1}{2B_u} \sum_{i=1}^{B_u} \mathbb{I}_i \left[H(p_{1,i}^{\text{sf}}, \hat{p}_{w,i}) + H(p_{2,i}^{\text{sf}}, \hat{p}_{w,i}) \right], \quad (5)$$

where B_u is the unlabeled batch size and $H(\cdot, \cdot)$ denotes the hard cross-entropy loss. The overall training objective of UniMatch v2 is then given by

$$\mathcal{L}_{\text{UniMatch v2}} = \mathcal{L}_{\text{sup}} + \lambda_u \mathcal{L}_{\text{u}}^{\text{v2}}, \quad (6)$$

where the teacher parameters are updated by EMA, $\theta_t \leftarrow \gamma\theta_t + (1 - \gamma)\theta_s$.

VESSA-Assisted Semi-Supervised Segmentation. We now describe how VESSA is integrated into UniMatch v2 during semi-supervised training for a downstream medical segmentation task. The overall framework is illustrated in Figure 2. At the beginning of training, all labeled images and their masks are inserted into the VESSA template bank. For each labeled sample (x^l, y^l) , the task-specific model follows the standard UniMatch v2 supervised path, producing the loss \mathcal{L}_{sup} defined in Eq. 4. The main challenge lies in utilizing the unlabeled set \mathcal{D}_u , where VESSA and UniMatch jointly provide complementary pseudo-label guidance.

Workflow. For an unlabeled image x^u , we follow VESSA’s inference procedure by selecting the top-3 visually similar templates from the template bank and sampling one according to the similarity-based distribution described in Eq. 1. The image x^u , its selected template overlay, and a reference text prompt are then fed into VESSA to produce a segmentation prediction $p_v = f_{\text{VESSA}}(x^u, x_{\text{temp}}, y_{\text{text}}^{\text{in}})$, which serves as VESSA’s pseudo-label.

Meanwhile, UniMatch v2 generates three complementary predictions. The weakly augmented view $x_w = A_w(x^u)$ is passed through the EMA teacher to obtain the weak pseudo-label $p_w = f_{\theta_t}(x_w)$. Two strongly augmented views, $x_{s1} = A_s(x_w)$ and $x_{s2} = A_s(x_w)$, are processed by a shared encoder g . Complementary channel-wise Dropout masks M and $1 - M$ are applied to their features, producing $e_{s1} = g(x_{s1}) \odot M \times 2$ and $e_{s2} = g(x_{s2}) \odot (1 - M) \times 2$, which are decoded into the strong-view predictions $p^{\text{sf}} = h(e_{s1})$ and $p^{\text{si}} = h(e_{s2})$.

Joint Supervision From vessa and the EMA Teacher. Unlike standard UniMatch v2, where the strong predictions p^{sf} and p^{si} are supervised only by the teacher’s p_w , we incorporate an additional and often more reliable supervision from vessa. Let $\hat{p}_w = \arg \max_c p_{w,c}$ and $\hat{p}_v = \arg \max_c p_{v,c}$ be the hard pseudo-labels from the teacher and vessa.

We define the VESSA supervision term as:

$$\mathcal{L}_{\text{vessa}} = H(p^{\text{sf}}, \hat{p}_v) + H(p^{\text{si}}, \hat{p}_v), \quad (7)$$

which captures the vessa-driven learning signal for both strong views.

The overall dual-source unsupervised objective becomes:

$$\begin{aligned} \mathcal{L}_{\text{u}}^{\text{joint}} = & \frac{1}{2B_u} \sum_{i=1}^{B_u} \mathbb{I}_i \left[\alpha_t (H(p_i^{\text{sf}}, \hat{p}_{w,i}) + H(p_i^{\text{si}}, \hat{p}_{w,i})) \right. \\ & \left. + \alpha_v \underbrace{(H(p_i^{\text{sf}}, \hat{p}_{v,i}) + H(p_i^{\text{si}}, \hat{p}_{v,i}))}_{\mathcal{L}_{\text{vessa}}} \right], \end{aligned} \quad (8)$$

where $\mathbb{I}_i = \mathbf{1}(\max_c p_{w,i,c} \geq \tau)$ is the teacher-derived confidence mask, and α_t, α_v control the relative strengths of teacher and vessa supervision.

Dynamic Weight Scheduling. Because the EMA teacher is weak at the beginning of training but improves over time, while VESSA provides stable and high-quality predictions from the start, we apply a simple scheduling strategy where the VESSA weight is set as $\alpha_v(t) = 1 - \eta(t)$ and the teacher weight as $\alpha_t(t) = \eta(t)$. Here, t denotes the training iteration and $\eta(t) \in [0, 1]$ is a monotonically increasing function (e.g., a cosine ramp-up). Thus, early in training $\alpha_v(t)$ dominates to exploit VESSA’s reliability, whereas later $\alpha_t(t)$ increases as the EMA teacher becomes more accurate.

Teacher-to-VESSA Feedback. To further refine VESSA during training, the EMA teacher also provides structural cues to VESSA. The teacher’s prediction p_w is converted into a spatial prompt embedding q_{prompt} (e.g., bounding boxes, point cues, or probability maps), which is injected into VESSA’s mask decoder to refine its output, i.e., $m_v = D_{\text{mask}}(p_{\text{VESSA}}, q_{\text{prompt}})$. This mutual learning allows VESSA to leverage evolving task-specific priors from the teacher, improving its inference quality and strengthening its supervisory role.

Overall Training Loss. The full optimization objective becomes:

$$\mathcal{L} = \mathcal{L}_{\text{sup}} + \lambda_u \mathcal{L}_{\text{u}}^{\text{joint}}. \quad (9)$$

where λ_u balances the contribution of unlabeled data. Through mutual reinforcement among VESSA, the EMA teacher, and the student model, each component progressively improves, resulting in stronger pseudo-labels and better downstream segmentation performance.

4. Experiments

We pretrain VESSA on seven public medical datasets spanning multiple anatomical regions—including cardiac, abdominal, brain, breast, and chest imaging—across four modalities (MRI, CT, ultrasound, and X-ray). Detailed dataset descriptions are provided in the supplementary material, and no dataset overlaps with those used for the training and validation of the task-specific semi-supervised learning frameworks. We evaluated our framework on two public datasets, covering cardiac MRI and abdominal CT organ segmentation tasks.

Dataset: The ACDC dataset [3] contains 150 cine short-axis cardiac MRI exams from five clinical subgroups, including normal, myocardial infarction, dilated cardiomyopathy, hypertrophic cardiomyopathy, and abnormal right ventricle. Each exam provides manual annotations for the left ventricle (LV), right ventricle (RV), and myocardium (MYO). Following common practice, we performed a patient-level 80/20 split for training and testing. The AbdomenCT-1K dataset [26] contains over 1,000 ab-

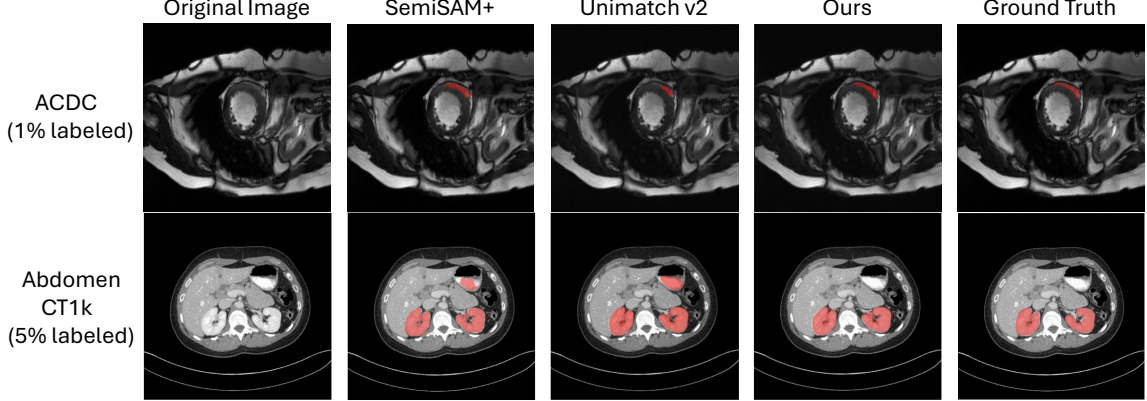


Figure 4. Comparison of the qualitative results on ACDC (1% labeled data setting) and AbdomenCT1k (5% labeled data setting)

Methods	RV	MYO	LV	Average
VESSA	0.731/0.819/39.12	0.822/0.852/19.21	0.828/0.875/27.64	0.793/0.849/28.65
UnimatchV2 + SAM2.1	0.623/0.752/37.76	0.134/0.548/16.85	0.740/0.839/6.38	0.499/0.713/20.33
Ours	0.773/0.846/20.24	0.855/0.876/13.46	0.845/0.889/17.05	0.824/0.870/16.92

Table 1. Ablation study on the ACDC dataset using 1% labeled data.

dominal CT scans from 12 medical centers, including both contrast-enhanced and non-contrast studies. Each scan is annotated for major abdominal organs such as liver, spleen, kidneys, and pancreas, with substantial appearance variability across institutions. For evaluation, we utilized CC scans for training and DD scans for testing.

Metrics: We evaluate performance using Dice score, Intersection-over-Union (IoU), and the 95th percentile Hausdorff Distance (HD95). Dice and IoU measure volumetric overlap from complementary perspectives, while HD95 assesses boundary accuracy. These three metrics together provide a compact yet comprehensive evaluation of region consistency and contour precision.

Implementation Details. Our method is implemented in PyTorch and trained on NVIDIA A100 GPUs (40GB and 80GB). VESSA uses DINOv2 [31] to extract both template features and input image features, Qwen3VL [38] as its vision-language backbone, and SAM 2.1 [34] as the segmentation backbone. UniMatch v2 [43] is adopted as the task-specific semi-supervised segmentation model, using DINOv2 as encoder and DPT [33] as decoder. For VESSA training, we follow its full configuration, including optimizer settings, input resolution, and augmentation strategies. For UniMatch v2 training with VESSA, we use the official recommended hyperparameters of UniMatch v2. For all comparison methods, including UniMatch v2 and SemiSAM+ [50], we also use their official released parameters for a fair evaluation.

Table 2. Segmentation performance comparison on the ACDC dataset. We compare our method with two recent state-of-the-art approaches, SemiSAM+ and UniMatch v2, under 1%, 5%, and 10% labeled data regimes. We report Dice/ IoU/ 95th-percentile Hausdorff distance (HD95) for each segmentation class and their average. Results obtained with 100% labeled data are also included as a fully supervised upper bound.

ACDC	cls	1%	5%	10%
SemiSAM+ [MIA'25] [50]	RV	0.759/0.644/21.86	0.819/0.728/8.76	0.830/0.747/6.98
	MYO	0.752/0.631/15.59	0.815/0.708/9.63	0.834/0.737/5.53
	LV	0.822/0.743/16.54	0.877/0.813/10.92	0.889/0.832/8.67
	AVG.	0.778/0.673/17.99	0.837/0.750/9.77	0.851/0.772/ 7.06
UniMatch-V2 [TPAMI'25] [43]	RV	0.693/0.811/23.03	0.833/0.879/13.15	0.841/0.880/13.69
	MYO	0.803/0.848/13.37	0.873/0.893/7.81	0.881/0.897/8.03
	LV	0.742/0.823/42.10	0.908/0.924/8.04	0.919/0.932/7.31
	AVG.	0.746/0.827/26.17	0.871/0.899/ 9.67	0.880/0.903/9.68
Ours	RV	0.773/0.846/20.24	0.835/0.879/15.03	0.860/0.891/11.84
	MYO	0.855/0.876/13.46	0.879/0.896/8.08	0.885/0.900/8.05
	LV	0.845/0.889/17.05	0.910/0.926/9.35	0.906/0.925/10.56
	AVG.	0.824/0.870/16.92	0.875/0.900/10.82	0.884/0.905/10.15
100%				
Supervised	RV		0.929/0.938/4.82	
	MYO		0.942/0.945/3.65	
	LV		0.955/0.959/3.97	
	MEAN		0.942/0.947/4.15	

4.1. Comparison with State-of-the-Art Methods

We compare our method with two strong semi-supervised baselines, UniMatch v2 and SemiSAM+, using their official configurations. We additionally evaluate one fully-supervised reference: an “upper bound” trained by treating all labeled and unlabeled images as labeled. For both fully-supervised settings, we adopt the same UniMatch v2

Table 3. Segmentation performance comparison on the AbdomenCT1k dataset. We compare our method with two recent state-of-the-art approaches, SemiSAM+ and UniMatch v2, under 1%, 5%, and 10% labeled data regimes. We report Dice/ IoU/ HD95 for each segmentation class and their average. Results obtained with 100% labeled data are also included as a fully supervised upper bound.

AbdomenCT	cls	1%	5%	10%
SemiSAM+ [MIA'25] [50]	Liver	0.784/0.710/95.06	0.854/0.798/60.76	0.880/0.826/49.83
	Kidney	0.763/0.669/58.19	0.875/0.812/29.89	0.880/0.819/30.45
	Spleen	0.606/0.526/104.07	0.790/0.735/66.23	0.845/0.791/44.66
	Pancreas	0.224/0.153/204.74	0.474/0.352/72.75	0.524/0.392/64.24
	AVG.	0.594/0.515/115.51	0.748/0.674/57.41	0.782/0.707/47.30
Unimatch-V2 [TPAMI'25] [43]	Liver	0.880/0.922/20.11	0.946/0.958/15.44	0.936/0.951/22.88
	Kidney	0.813/0.877/70.35	0.870/0.910/37.84	0.896/0.926/21.98
	Spleen	0.622/0.780/41.12	0.884/0.926/12.20	0.904/0.934/11.12
	Pancreas	0.171/0.559/80.24	0.494/0.695/45.17	0.620/0.745/45.75
	AVG.	0.622/0.784/52.96	0.798/0.872/27.66	0.839/0.889/25.43
Ours	Liver	0.867/0.913/48.12	0.946/0.924/13.28	0.927/0.947/22.06
	Kidney	0.878/0.910/38.32	0.931/0.944/19.18	0.931/0.944/17.22
	Spleen	0.836/0.894/15.33	0.860/0.911/15.37	0.885/0.923/27.19
	Pancreas	0.459/0.670/68.96	0.546/0.713/50.43	0.613/0.743/44.98
	AVG.	0.760/0.847/42.68	0.821/0.873/24.57	0.839/0.889/27.86
100%				
Supervised	Liver	0.970/0.974/3.69		
	Kidney	0.958/0.961/3.56		
	Spleen	0.947/0.958/5.64		
	Pancreas	0.928/0.937/4.31		
	AVG.	0.951/0.958/4.30		

architecture (DINOv2 encoder and DPT decoder) to ensure a fair comparison.

Experiments are conducted on two datasets: ACDC and AbdomenCT1k. For each dataset, we evaluate under 1%, 5%, and 10% labeled data, and report Dice, IoU, and HD95 for each class as well as the class-wise mean. Quantitative results across all label ratios are summarized in Table 2 and Table 3.

Quantitative Results. Across all datasets, our method consistently outperforms UniMatch v2 and SemiSAM+, with the largest gains observed under extremely limited supervision (1%–5% labels). These results highlight the reliability of VESSA-generated pseudo-labels when annotations are scarce. As the labeled ratio increases (e.g., 10%), the performance gap naturally narrows because the student network itself becomes stronger and provides more accurate guidance to VESSA. In such cases, both UniMatch v2 and our VESSA-assisted model approach similarly high performance, and further expanding the template bank does not necessarily yield better template matches. Nevertheless, in the challenging low-label regime, our framework delivers substantial improvements, effectively pushing the limits of semi-supervised medical image segmentation.

Qualitative Results. Figure 4 presents qualitative comparisons on ACDC and AbdomenCT1k. Our approach produces more reliable boundaries, more coherent structures, and more smooth delineations of fine anatomical details

compared with UniMatch v2 and SemiSAM+. These improvements are especially evident in the challenging samples where the organs are very small or the boundaries are blurred. Additional qualitative examples and dataset-specific analyses are provided in the supplementary material.

4.2. Ablation Study

Effectiveness of VESSA within the Proposed Framework.

To assess the contribution of VESSA, we compare our full framework against a variant in which SAM is directly used to generate pseudo-labels for the UniMatch V2 specialist model. For a fair comparison, we adopt the same interaction protocol between UniMatch v2 and SAM2 as in our method. On ACDC with 1% labeled data, our framework consistently and substantially outperforms the SAM-supervised baseline across all anatomical structures. These results indicate that VESSA produces markedly higher-quality pseudo-labels than SAM, which in turn leads to stronger semi-supervised segmentation performance.

Effectiveness of the Task-Specific Semi-Supervised Model.

To evaluate the importance of task-specific semi-supervised learning, we further compare our full framework with a VESSA-only variant, where VESSA performs inference solely using its template bank, without exploiting unlabeled data or UniMatch v2. On ACDC with 1% labeled data, our method achieves clear improvements across all organ classes. This demonstrates that coupling VESSA with a task-specific semi-supervised learner, together with mutual learning between VESSA and UniMatch v2, is crucial for obtaining high segmentation accuracy.

We summarize the ablation results in Table 1, where we compare our method with (i) VESSA alone and (ii) UniMatch v2 combined with SAM2. Additional ablation studies, including the effect of student-to-VESSA prompting during training of the task-specific semi-supervised framework and the impact of individual components in VESSA’s training, are provided in the supplementary material.

5. Conclusion

In this work, we introduced VESSA, a vision–language foundation model designed for semi-supervised medical image segmentation, and demonstrated its effective integration with a task-specific learner via a unified training framework. Through template-guided prompting, visual–text alignment, and memory-driven decoding, VESSA generates high-quality pseudo-labels that enhance supervision under limited annotations. We further showed that combining VESSA with UniMatch v2 [43] via mutual learning yields complementary benefits: VESSA offers strong structural priors early on, while the student model provides

task-adaptive feedback to refine VESSA’s predictions. Experiments on two benchmark medical datasets under label-scarce settings confirm the robustness and effectiveness of our approach. This work highlights a promising direction for unifying foundation models with specialized learners toward scalable, label-efficient medical segmentation.

Vision–Language Enhanced Foundation Model for Semi-supervised Medical Image Segmentation

Supplementary Material

6. Pre-training Data of VESSA

To build a modality-agnostic medical foundation model, VESSA is pre-trained on a diverse collection of publicly available datasets spanning multiple imaging modalities and anatomical regions. This heterogeneous pre-training corpus enables the model to acquire robust structural priors and modality-invariant representations across CT, MRI, X-ray, and ultrasound. The datasets used are summarized below:

- **AMOS22**[14]: The AMOS22 dataset comprises 500 abdominal CT volumes and 100 MRI volumes, featuring voxel-level annotations for 15 abdominal organs. These include the spleen, right and left kidneys, gallbladder, esophagus, liver, stomach, aorta, inferior vena cava (IVC), pancreas, right and left adrenal glands, duodenum, bladder, and prostate/uterus.
- **LGG**[4]: The LGG dataset contains 110 multi-modal MRI studies (T1, T1c, T2, FLAIR). It provides binary segmentation masks for tumor delineation.
- **M&Ms**[5]: This dataset includes 375 short-axis cardiac cine MRI sequences from multiple centers and vendors. Classes cover left ventricle, right ventricle, and myocardium.
- **CAMUS**[19]: CAMUS offers 2,000 2D echocardiography images and 120 3D sequences. Classes include LV endocardium and LV myocardium, and left atrium..
- **ChestXray**[13]: This dataset contains 896 chest radiographs with pixel-level instance segmentation annotations. It covers two clinical conditions: healthy lungs and tuberculosis-infected lungs.
- **BUSI**[1]: BUSI contains 780 breast ultrasound images categorized into three classes: normal, benign, and malignant. Segmentation masks are provided for lesion delineation.

For all of these datasets, we adopt the original split method as in the BiomedParseData[51]. Together, these datasets cover a wide range of imaging physics, anatomical structures, and clinical acquisition protocols, enabling VESSA to learn transferable representations that generalize effectively to downstream semi-supervised medical image segmentation tasks.

7. Augmentation Method of Template Images for the Training of VESSA

VESSA employs a dedicated augmentation module applied to template images and their corresponding masks. The augmentation is performed on tensor inputs and consists of

the following transformations:

- **Geometric Transformations (image & mask):** random horizontal/vertical flipping, rotations, and random cropping with a scale range of (0.7, 1.0), followed by resizing back to the original resolution.
- **Photometric Transformations (image only):** random Gaussian and random sharpening.
- **Resolution Restoration:** images are resized via bilinear interpolation, while masks use nearest-neighbor interpolation to preserve discrete label boundaries.

8. Additional Qualitative Results

Figure 5 presents additional qualitative comparisons on all ACDC [3] segmentation classes, left ventricle (LV), right ventricle (RV), and myocardium (MYO), using models trained with only 1% labeled data. As shown in the visualizations, our method consistently produces more precise boundaries and more anatomically coherent structures than both SemiSAM+ [50] and Unimatch v2 [43]. Across all classes, the predicted contours from our model closely align with the ground-truth shapes, whereas the SemiSAM+ and Unimatch v2 often exhibit notable over-segmentation or “hallucination,” incorrectly assigning labels to regions outside the target anatomy. SemiSAM+ shows such errors across LV, RV, and MYO, while Unimatch v2 displays over-segmentation primarily in the LV. In contrast, our method avoids these failure modes entirely and yields the most accurate and structurally faithful predictions.

Figure 6 provides further qualitative comparisons on AbdomenCT-1K [26] for four abdominal organs: liver, kidneys, spleen, and pancreas. The visualizations show that our method produces cleaner boundaries and more coherent organ shapes than SemiSAM+ and Unimatch v2 across all classes. Both SemiSAM+ and Unimatch v2 frequently exhibit over-segmentation or hallucinated regions—particularly for the liver, kidneys, and spleen—likely due to the presence of tissues with similar texture, contrast, or morphology. Although SemiSAM+ and Unimatch v2 avoid strong over-segmentation on the pancreas, SemiSAM+ still outlines non-pancreatic structures with incorrect contours. In all cases, our method demonstrates the most stable and anatomically precise predictions, with no observable over-segmentation artifacts.

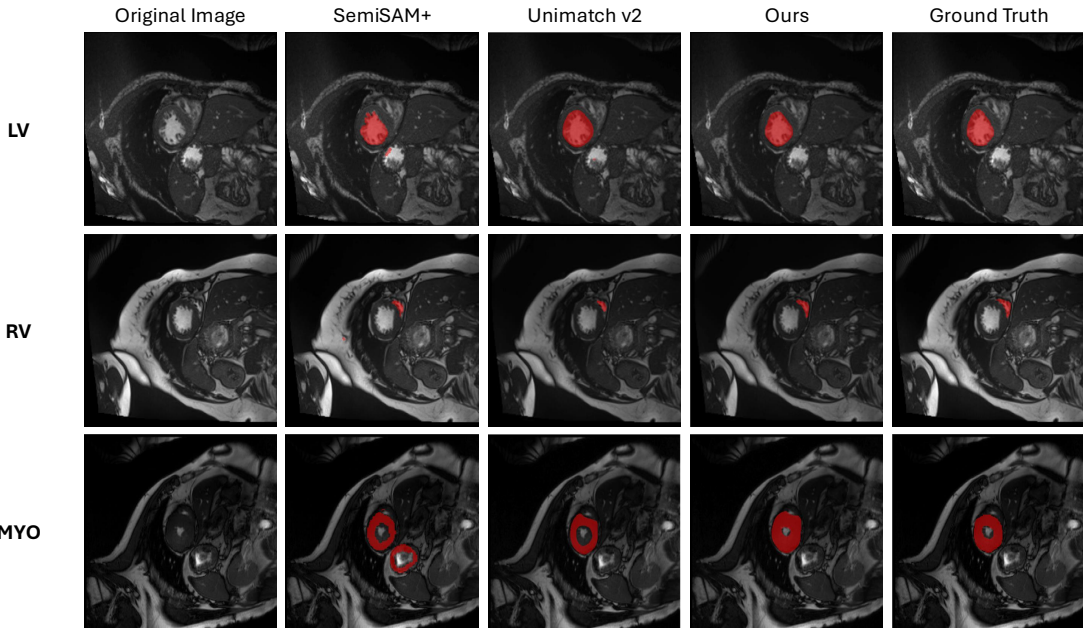


Figure 5. Comparison of the qualitative results on all segmentation classes of ACDC (1% labeled data setting)

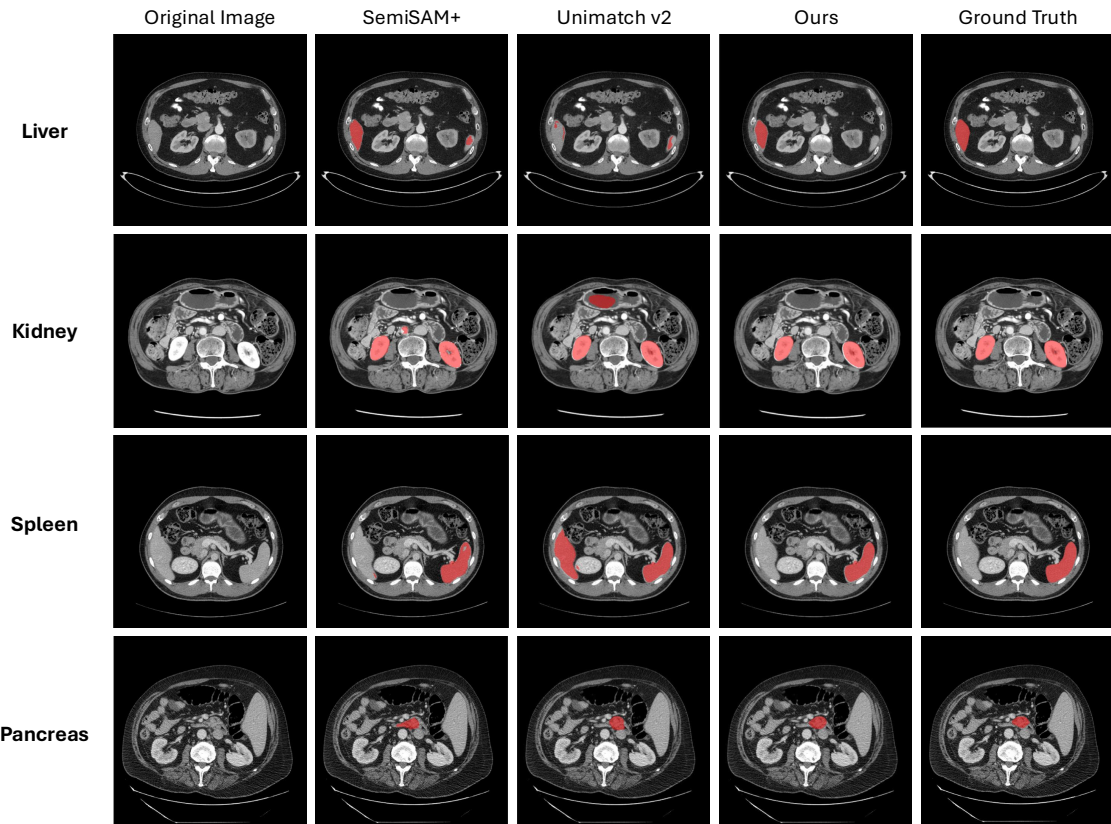


Figure 6. Comparison of the qualitative results on all segmentation classes of AbdomenCT1k (1% labeled data setting)

9. Additional Ablation Studies

This section presents additional ablation studies, organized according to the two stages of our framework: Stage 1, in which VESSA is pre-trained as a reference-guided segmentation assistant, and Stage 2, in which VESSA is integrated into the task-specific semi-supervised segmentation framework. Subsection 1 evaluates the contribution of the individual components within VESSA, and Subsection 2 analyzes the effect of the proposed student-to-VESSA prompting mechanism during Stage 2 training.

9.1. Effectiveness of Individual Components in VESSA

We first study the contribution of two key components in VESSA—the VLM-based semantic prompting module and the memory mechanism. For each component, we briefly recap its functional role and then describe the corresponding ablation setup and its impact on performance.

During both training and inference, the VLM receives a prompt comprising the input image, the matched template overlay, and the reference text. The VLM produces a $< SEG >$ token, which is projected through an MLP to form the semantic prompt embedding fed into the prompt encoder of the segmentation foundation model. To evaluate the role of the VLM, we remove this semantic embedding entirely. In this setting, only the input image is fed to the image encoder, and only the matched template and its annotation are provided to the memory encoder. The resulting performance is reported in the “w/o VLM” columns of Table 4 and Table 5 for ACDC and AbdomenCT-1K (1% labeled setting). Across all classes and both datasets, removing the VLM causes substantial performance degradation after Stage 1 pre-training and during subsequent semi-supervised training, demonstrating the importance of VLM-derived semantic prompting.

In VESSA, the matched template and its annotations are encoded by the memory encoder to generate template-conditioned features, which interact with the image features via cross-attention before being passed to the mask decoder. For the ablation, we remove the memory encoder input entirely, eliminating template-conditioned memory features. Results under this configuration are reported in the “w/o memory” columns of Table 4 and Table 5. The absence of the memory mechanism leads to drops in Dice performance on both datasets, with the decline particularly pronounced on the more challenging AbdomenCT-1K dataset. These results confirm that memory-guided feature conditioning is crucial to the effectiveness of VESSA.

9.2. Effectiveness of Student-to-VESSA Prompting during Training of Task-specific Semi-supervised Segmentation

We further evaluate the contribution of our student-to-VESSA prompting mechanism introduced in Stage 2. The motivation behind this design is that, as training progresses, the student model becomes increasingly accurate under the supervision of both the teacher branch and VESSA. In the later training stages, the student’s predictions often surpass VESSA in spatial precision. Feeding these refined student predictions back into VESSA as spatial/location prompts enables VESSA to continually improve its pseudo-label quality, creating a mutually reinforcing feedback loop between VESSA and the student model.

Importantly, in more challenging datasets where VESSA’s standalone inference performance is less reliable during semi-supervised training, the student-to-VESSA prompting mechanism plays a critical role. This is reflected by the larger performance drop on the AbdomenCT-1K dataset when student-to-VESSA prompting is removed in Table 5, indicating that dynamic conditioning on student predictions is essential for stabilizing and improving VESSA’s guidance in difficult imaging scenarios.

To assess this mechanism, we disable student-to-VESSA prompting, forcing VESSA to generate static pseudo-labels throughout training. The performance of this configuration is listed in the “w/o student” columns of Table 4 and Table 5. Across both ACDC and AbdomenCT-1K (1% labeled), removing student-to-VESSA prompting leads to consistent performance drops, confirming that dynamically conditioning VESSA on the increasingly reliable student predictions is an essential component of our Stage 2 training strategy.

Region	w/o VLM	w/o memory	w/o student	Ours
RV	0.560	0.776	0.751	0.773
MYO	0.642	0.824	0.832	0.855
LV	0.612	0.860	0.862	0.845
AVE	0.604	0.820	0.815	0.824

Table 4. Dice comparison on ACDC under 1% setting.

Organ	w/o VLM	w/o memory	w/o student	Ours
Liver	0.482	0.566	0.849	0.867
Kidney	0.822	0.883	0.847	0.878
Spleen	0.523	0.508	0.748	0.836
Pancreas	0.132	0.473	0.386	0.459
AVE	0.490	0.608	0.708	0.760

Table 5. Dice comparison on AbdomenCT1k under 1% setting.

References

[1] Walid Al-Dhabayani, Mohammed Gomaa, Hussien Khaled, and Aly Fahmy. Dataset of breast ultrasound images. *Data in brief*, 28:104863, 2020. [1](#)

[2] Eric Arazo, Diego Ortego, Paul Albert, Noel E O'Connor, and Kevin McGuinness. Pseudo-labeling and confirmation bias in deep semi-supervised learning. In *2020 International joint conference on neural networks (IJCNN)*, pages 1–8. IEEE, 2020. [2](#)

[3] Olivier Bernard, Alain Lalande, Clement Zotti, Frederick Cervenansky, Xin Yang, Pheng-Ann Heng, Irem Cetin, Karim Lekadir, Oscar Camara, Miguel Angel Gonzalez Ballester, et al. Deep learning techniques for automatic mri cardiac multi-structures segmentation and diagnosis: is the problem solved? *IEEE transactions on medical imaging*, 37(11):2514–2525, 2018. [1, 6](#)

[4] Mateusz Buda, Ashirbani Saha, and Maciej A Mazurowski. Association of genomic subtypes of lower-grade gliomas with shape features automatically extracted by a deep learning algorithm. *Computers in biology and medicine*, 109:218–225, 2019. [1](#)

[5] Victor M Campello, Polyxeni Gkontra, Cristian Izquierdo, Carlos Martin-Isla, Alireza Sojoudi, Peter M Full, Klaus Maier-Hein, Yao Zhang, Zhiqiang He, Jun Ma, et al. Multi-centre, multi-vendor and multi-disease cardiac segmentation: the m&ms challenge. *IEEE Transactions on Medical Imaging*, 40(12):3543–3554, 2021. [1](#)

[6] Paola Cascante-Bonilla, Fuwen Tan, Yanjun Qi, and Vicente Ordóñez. Curriculum labeling: Revisiting pseudo-labeling for semi-supervised learning. In *Proceedings of the AAAI conference on artificial intelligence*, pages 6912–6920, 2021. [2](#)

[7] Xiaokang Chen, Yuhui Yuan, Gang Zeng, and Jingdong Wang. Semi-supervised semantic segmentation with cross pseudo supervision. In *Proceedings of the IEEE/CVF conference on computer vision and pattern recognition*, pages 2613–2622, 2021. [2](#)

[8] Ian Goodfellow, Jean Pouget-Abadie, Mehdi Mirza, Bing Xu, David Warde-Farley, Sherjil Ozair, Aaron Courville, and Yoshua Bengio. Generative adversarial networks. *Communications of the ACM*, 63(11):139–144, 2020. [2](#)

[9] Kai Han, Victor S Sheng, Yuqing Song, Yi Liu, Chengjian Qiu, Siqi Ma, and Zhe Liu. Deep semi-supervised learning for medical image segmentation: A review. *Expert Systems with Applications*, 245:123052, 2024. [1, 2](#)

[10] Yongsong Huang, Wanqing Xie, Mingzhen Li, Ethan Xiao, Jane You, and Xiaofeng Liu. Source-free domain adaptive segmentation with class-balanced complementary self-training. *Artificial Intelligence in Medicine*, 146:102694, 2023. [2](#)

[11] Wei-Chih Hung, Yi-Hsuan Tsai, Yan-Ting Liou, Yen-Yu Lin, and Ming-Hsuan Yang. Adversarial learning for semi-supervised semantic segmentation. *arXiv preprint arXiv:1802.07934*, 2018. [2](#)

[12] Fabian Isensee, Jens Petersen, Andre Klein, David Ziemer, Paul F Jaeger, Simon Kohl, Jakob Wasserthal, Gregor Koehler, Tobias Norajitra, Sebastian Wirkert, et al. nnu-net: Self-adapting framework for u-net-based medical image segmentation. *arXiv preprint arXiv:1809.10486*, 2018. [1](#)

[13] Stefan Jaeger, Sema Candemir, Sameer Antani, Yi-Xiáng J Wáng, Pu-Xuan Lu, and George Thoma. Two public chest x-ray datasets for computer-aided screening of pulmonary diseases. *Quantitative imaging in medicine and surgery*, 4(6):475, 2014. [1](#)

[14] Yuanfeng Ji, Haotian Bai, Jie Yang, Chongjian Ge, Ye Zhu, Ruimao Zhang, Zhen Li, Lingyan Zhang, Wanling Ma, Xiang Wan, et al. Amos: A large-scale abdominal multi-organ benchmark for versatile medical image segmentation. *arXiv preprint arXiv:2206.08023*, 2022. [1](#)

[15] Alexander Kirillov, Eric Mintun, Nikhila Ravi, Hanzi Mao, Chloe Rolland, Laura Gustafson, Tete Xiao, Spencer Whitehead, Alexander C Berg, Wan-Yen Lo, et al. Segment anything. In *Proceedings of the IEEE/CVF international conference on computer vision*, pages 4015–4026, 2023. [2, 3](#)

[16] Donghyeon Kwon and Suha Kwak. Semi-supervised semantic segmentation with error localization network. In *Proceedings of the IEEE/CVF conference on computer vision and pattern recognition*, pages 9957–9967, 2022. [2](#)

[17] Xin Lai, Zhuotao Tian, Yukang Chen, Yanwei Li, Yuhui Yuan, Shu Liu, and Jiaya Jia. Lisa: Reasoning segmentation via large language model. In *Proceedings of the IEEE/CVF Conference on Computer Vision and Pattern Recognition*, pages 9579–9589, 2024. [2, 3](#)

[18] Samuli Laine and Timo Aila. Temporal ensembling for semi-supervised learning. *arXiv preprint arXiv:1610.02242*, 2016. [2](#)

[19] Sarah Leclerc, Erik Smistad, Joao Pedrosa, Andreas Østvik, Frederick Cervenansky, Florian Espinosa, Torvald Espeland, Erik Andreas Rye Berg, Pierre-Marc Jodoin, Thomas Grennier, et al. Deep learning for segmentation using an open large-scale dataset in 2d echocardiography. *IEEE transactions on medical imaging*, 38(9):2198–2210, 2019. [1](#)

[20] Shuailin Li, Chuyu Zhang, and Xuming He. Shape-aware semi-supervised 3d semantic segmentation for medical images. In *International Conference on Medical Image Computing and Computer-Assisted Intervention*, pages 552–561. Springer, 2020. [1, 2](#)

[21] Yiwei Li, Yikang Liu, Jiaqi Guo, Lin Zhao, Zheyuan Zhang, Xiao Chen, Boris Mailhe, Ankush Mukherjee, Terrence Chen, and Shanhai Sun. Rau: Reference-based anatomical understanding with vision language models. *arXiv preprint arXiv:2509.22404*, 2025. [4](#)

[22] Geert Litjens, Thijs Kooi, Babak Ehteshami Bejnordi, Arnaud Arindra Adiyoso Setio, Francesco Ciompi, Mohsen Ghafoorian, Jeroen Awm Van Der Laak, Bram Van Ginneken, and Clara I Sánchez. A survey on deep learning in medical image analysis. *Medical image analysis*, 42:60–88, 2017. [1](#)

[23] Jin Liu, Huiyuan Fu, Chuanming Wang, and Huadong Ma. Region-aware exposure consistency network for mixed exposure correction. In *Proceedings of the AAAI Conference on Artificial Intelligence*, pages 3648–3656, 2024. [3](#)

[24] Timo Lüddecke and Alexander Ecker. Image segmentation using text and image prompts. In *Proceedings of*

the IEEE/CVF conference on computer vision and pattern recognition, pages 7086–7096, 2022. 2

[25] Xiangde Luo, Minhao Hu, Tao Song, Guotai Wang, and Shaoting Zhang. Semi-supervised medical image segmentation via cross teaching between cnn and transformer. In *International conference on medical imaging with deep learning*, pages 820–833. PMLR, 2022. 1, 2

[26] Jun Ma, Yao Zhang, Song Gu, Cheng Zhu, Cheng Ge, Yichi Zhang, Xingle An, Congcong Wang, Qiyuan Wang, Xin Liu, et al. Abdomenct-1k: Is abdominal organ segmentation a solved problem? *IEEE Transactions on Pattern Analysis and Machine Intelligence*, 44(10):6695–6714, 2021. 6, 1

[27] Jun Ma, Yuting He, Feifei Li, Lin Han, Chenyu You, and Bo Wang. Segment anything in medical images. *Nature Communications*, 15(1):654, 2024. 3

[28] Bjoern H Menze, Andras Jakab, Stefan Bauer, Jayashree Kalpathy-Cramer, Keyvan Farahani, Justin Kirby, Yuliya Burren, Nicole Porz, Johannes Slotboom, Roland Wiest, et al. The multimodal brain tumor image segmentation benchmark (brats). *IEEE transactions on medical imaging*, 34(10):1993–2024, 2014. 1

[29] Takeru Miyato, Shin-ichi Maeda, Masanori Koyama, and Shin Ishii. Virtual adversarial training: a regularization method for supervised and semi-supervised learning. *IEEE transactions on pattern analysis and machine intelligence*, 41(8):1979–1993, 2018. 2

[30] Ziwei Niu, Shuyi Ouyang, Shiao Xie, Yen-wei Chen, and Lanfen Lin. A survey on domain generalization for medical image analysis. *arXiv preprint arXiv:2402.05035*, 2024. 1

[31] Maxime Oquab, Timothée Darcet, Théo Moutakanni, Huy Vo, Marc Szafraniec, Vasil Khalidov, Pierre Fernandez, Daniel Haziza, Francisco Massa, Alaaeldin El-Nouby, et al. Dinov2: Learning robust visual features without supervision. *arXiv preprint arXiv:2304.07193*, 2023. 2, 3, 4, 7

[32] Alec Radford, Jong Wook Kim, Chris Hallacy, Aditya Ramesh, Gabriel Goh, Sandhini Agarwal, Girish Sastry, Amanda Askell, Pamela Mishkin, Jack Clark, et al. Learning transferable visual models from natural language supervision. In *International conference on machine learning*, pages 8748–8763. PMLR, 2021. 2

[33] René Ranftl, Alexey Bochkovskiy, and Vladlen Koltun. Vision transformers for dense prediction. In *Proceedings of the IEEE/CVF international conference on computer vision*, pages 12179–12188, 2021. 7

[34] Nikhila Ravi, Valentin Gabeur, Yuan-Ting Hu, Ronghang Hu, Chaitanya Ryali, Tengyu Ma, Haitham Khedr, Roman Rädle, Chloe Rolland, Laura Gustafson, et al. Sam 2: Segment anything in images and videos. *arXiv preprint arXiv:2408.00714*, 2024. 3, 4, 7

[35] Olaf Ronneberger, Philipp Fischer, and Thomas Brox. U-net: Convolutional networks for biomedical image segmentation. In *International Conference on Medical image computing and computer-assisted intervention*, pages 234–241. Springer, 2015. 1

[36] Kihyuk Sohn, David Berthelot, Nicholas Carlini, Zizhao Zhang, Han Zhang, Colin A Raffel, Ekin Dogus Cubuk, Alexey Kurakin, and Chun-Liang Li. Fixmatch: Simplifying semi-supervised learning with consistency and confidence. *Advances in neural information processing systems*, 33:596–608, 2020. 2, 5

[37] Antti Tarvainen and Harri Valpola. Mean teachers are better role models: Weight-averaged consistency targets improve semi-supervised deep learning results. *Advances in neural information processing systems*, 30, 2017. 1, 2, 5

[38] Qwen Team. Qwen3-vl: Vision-language model by qwen. <https://github.com/QwenLM/Qwen3-VL>, 2024. Accessed: 2025-01-01. 2, 7

[39] Vikas Verma, Kenji Kawaguchi, Alex Lamb, Juho Kannala, Arno Solin, Yoshua Bengio, and David Lopez-Paz. Interpolation consistency training for semi-supervised learning. *Neural Networks*, 145:90–106, 2022. 2

[40] Zhongwei Wan, Che Liu, Mi Zhang, Jie Fu, Benyou Wang, Sibo Cheng, Lei Ma, César Quilodrán-Casas, and Rossella Arcucci. Med-unic: Unifying cross-lingual medical vision-language pre-training by diminishing bias. *Advances in Neural Information Processing Systems*, 36:56186–56197, 2023. 2

[41] Risheng Wang, Tao Lei, Ruixia Cui, Bingtao Zhang, Hongying Meng, and Asoke K Nandi. Medical image segmentation using deep learning: A survey. *IET image processing*, 16(5):1243–1267, 2022. 1, 2

[42] Lihe Yang, Lei Qi, Litong Feng, Wayne Zhang, and Yinghuan Shi. Revisiting weak-to-strong consistency in semi-supervised semantic segmentation. In *Proceedings of the IEEE/CVF conference on computer vision and pattern recognition*, pages 7236–7246, 2023. 1, 2

[43] Lihe Yang, Zhen Zhao, and Hengshuang Zhao. Unimatch v2: Pushing the limit of semi-supervised semantic segmentation. *IEEE Transactions on Pattern Analysis and Machine Intelligence*, 2025. 3, 5, 7, 8, 1

[44] Xiangli Yang, Zixing Song, Irwin King, and Zenglin Xu. A survey on deep semi-supervised learning. *IEEE transactions on knowledge and data engineering*, 35(9):8934–8954, 2022. 1

[45] Lequan Yu, Shujun Wang, Xiaomeng Li, Chi-Wing Fu, and Pheng-Ann Heng. Uncertainty-aware self-ensembling model for semi-supervised 3d left atrium segmentation. In *International conference on medical image computing and computer-assisted intervention*, pages 605–613. Springer, 2019. 1, 2

[46] Chaoning Zhang, Joseph Cho, Fachrina Dewi Puspitasari, Sheng Zheng, Chenghao Li, Yu Qiao, Taegoo Kang, Xinru Shan, Chenshuang Zhang, Caiyan Qin, et al. A survey on segment anything model (sam): Vision foundation model meets prompt engineering. *arXiv preprint arXiv:2306.06211*, 2023. 2

[47] Yuhao Zhang, Hang Jiang, Yasuhide Miura, Christopher D Manning, and Curtis P Langlotz. Contrastive learning of medical visual representations from paired images and text. In *Machine learning for healthcare conference*, pages 2–25. PMLR, 2022. 2

[48] Yichi Zhang, Shiyao Hu, Sijie Ren, Chen Jiang, Yuan Cheng, and Yuan Qi. Enhancing the reliability of segment anything model for auto-prompting medical image segmentation with

uncertainty rectification. *arXiv preprint arXiv:2311.10529*, 2023. [2](#)

[49] Yichi Zhang, Jin Yang, Yuchen Liu, Yuan Cheng, and Yuan Qi. Semisam: Enhancing semi-supervised medical image segmentation via sam-assisted consistency regularization. In *2024 IEEE International Conference on Bioinformatics and Biomedicine (BIBM)*, pages 3982–3986. IEEE, 2024. [3](#)

[50] Yichi Zhang, Bohao Lv, Le Xue, Wenbo Zhang, Yuchen Liu, Yu Fu, Yuan Cheng, and Yuan Qi. Semisam+: Rethinking semi-supervised medical image segmentation in the era of foundation models. *arXiv preprint arXiv:2502.20749*, 2025. [3, 7, 8, 1](#)

[51] Theodore Zhao, Yu Gu, Jianwei Yang, Naoto Usuyama, Ho Hin Lee, Sid Kiblawi, Tristan Naumann, Jianfeng Gao, Angela Crabtree, Jacob Abel, et al. A foundation model for joint segmentation, detection and recognition of biomedical objects across nine modalities. *Nature methods*, 22(1):166–176, 2025. [1](#)

[52] Yongfa Zhu, Xue Wang, Taihui Liu, and Yongkang Fu. Multi-perspective dynamic consistency learning for semi-supervised medical image segmentation. *Scientific Reports*, 15(1):18266, 2025. [3](#)

[53] Xueyan Zou, Jianwei Yang, Hao Zhang, Feng Li, Linjie Li, Jianfeng Wang, Lijuan Wang, Jianfeng Gao, and Yong Jae Lee. Segment everything everywhere all at once. *Advances in neural information processing systems*, 36:19769–19782, 2023. [2](#)